Characterizing Jupiter's Interior Using Machine Learning:

From a Multidimensional Problem to Four Key Structures

Maayan Ziv[1], Eli Galanti[1], Saburo Howard[2], Tristan Guillot[3], and Yohai Kaspi[1]

[1]Department of Earth and Planetary Sciences, Weizmann Institute of Science, Rehovot, Israel,
[2]Institut für Astrophysik, Universität Zürich, Switzerland, [3]Observatoire de la Côte d'Azur, Nice, France

maayan.ziv@weizmann.ac.il

NeuralCMS paper

Full exploration paper

Key points

- **Jupiter's interior structure** is constrained by Juno's gravity measurements, Galileo probe atmospheric data, and Voyager's radio occultations
- **NeuralCMS**, a deep neural network model, computes interior structures based on the accurate concentric Maclaurin spheroids (CMS) method (Hubbard 2013)
- The interior model is coupled to a **wind model**, enabling a consistent approach for selecting and characterizing plausible interior structures
- Clustering analysis identifies **four key interior structures** for Jupiter, simplifying the problem to two effective parameters
- The **most observationally constrained models** fall within one of the key structures
- Galileo's atmospheric data may not represent the entire envelope of Jupiter

Jupiter's interior structure model

$$J_n = -\frac{1}{R_{\mathrm{eq}}{}^n M}\int r^n P_n(\sin\theta)\,\rho(r,\theta)\,d^3r$$

J_n: Observation; $\rho(r,\theta)$: Model

- Four-layer models of Jupiter with $N = 1041$ spheroids.
- Seven controlling parameters.
- State-of-the-art EOS for H-He: HG23+CMS19.

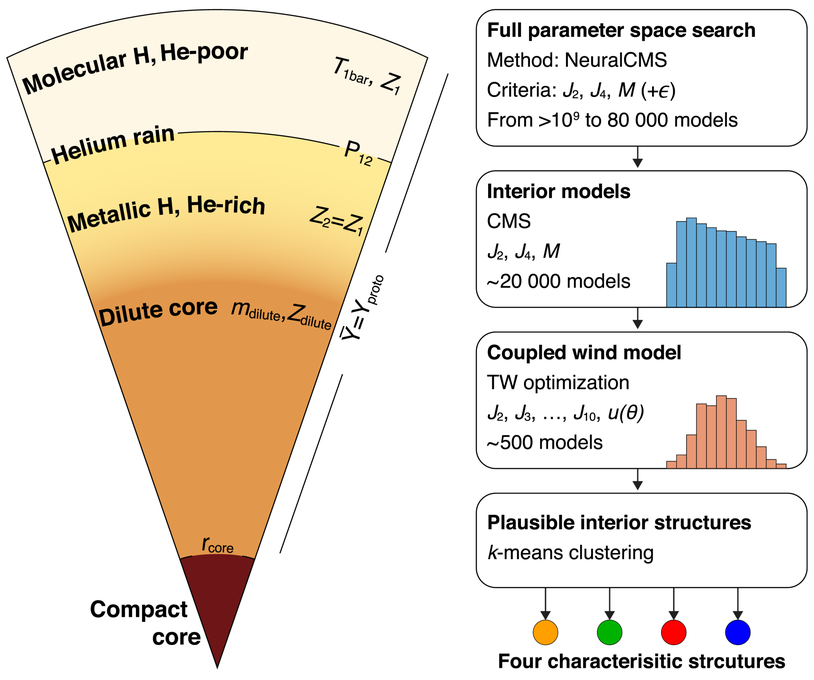

Figure 1 Schematic view of Jupiter's interior model (*left*) and the exploration workflow (*right*). NeuralCMS and CMS accepts models with a wide range for J_2 and J_4, and the thermal wind model (TW) constrain all even and odd gravity harmonics (J_n) to Juno's 3σ uncertainty.

Exploration with NeuralCMS

- Regression of the CMS model with a reduced run time by a factor of ~10^5
- Takes the seven interior parameters as input to predict J_2, J_4, J_6, J_8, and M
- Grid search iterations generate a large sample of plausible interior models

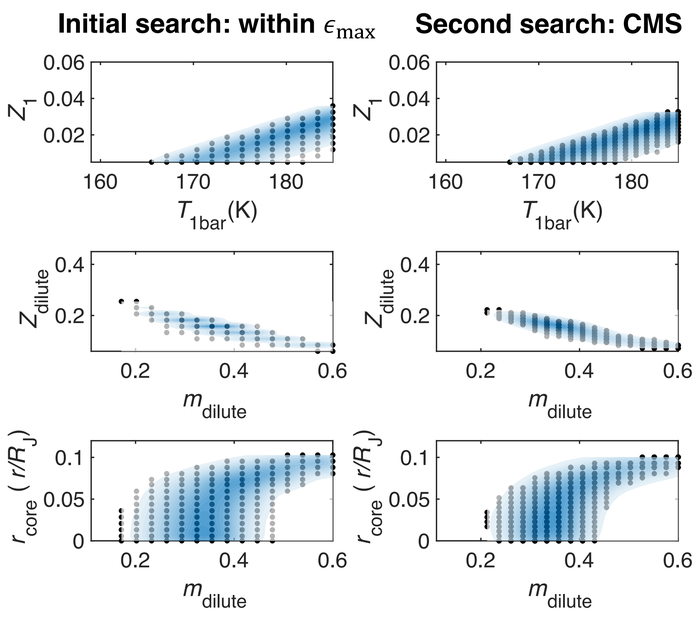

Figure 2 The left column shows accepted models predicted by NeuralCMS in the first grid search, within the NeuralCMS maximal absolute prediction errors on the validation dataset. In the right column are accepted models computed with CMS found in the second tighter grid search. The axes range is the initial wide search range.

Coupling the interior to a wind model

$$2\Omega r\frac{\partial}{\partial z}(\rho_{\mathrm{static}}u) = g_{\mathrm{static}}\frac{\partial \rho'}{\partial \theta}$$

Interior solution — wind model

- Thermal wind (TW) balance relates solid-body (static) solutions to the wind
- Optimize the cloud level wind and its decay (Galanti+ 2019)
- Fit all J_2-J_{10} to Juno 3σ uncertainty (Durante+2020)
- Within ± 20 m/s of the observed wind (Tollefson+2017)

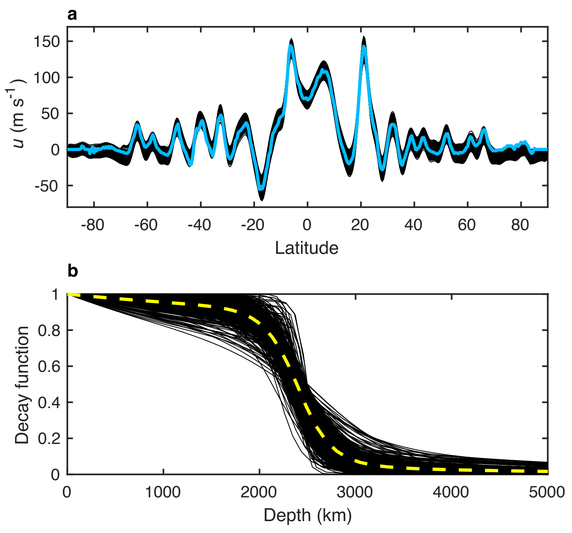

Figure 3 Optimized wind solutions for all ~500 plausible model. *Panel a*: latitudinal cloud-level wind profiles. *Panel b*: the radial decay function with depth. The blue profile represents the observed cloud-level wind (Tollefson+2017), and the dashed yellow profile indicates the mean of all decay profiles.

Results 1: Distribution of plausible structures

- The wind model considerbly constrain the low-order gravity harmonics J_2 and J_4
- The distribution of interior parameters is more refined but does not change significantly by wind constraints

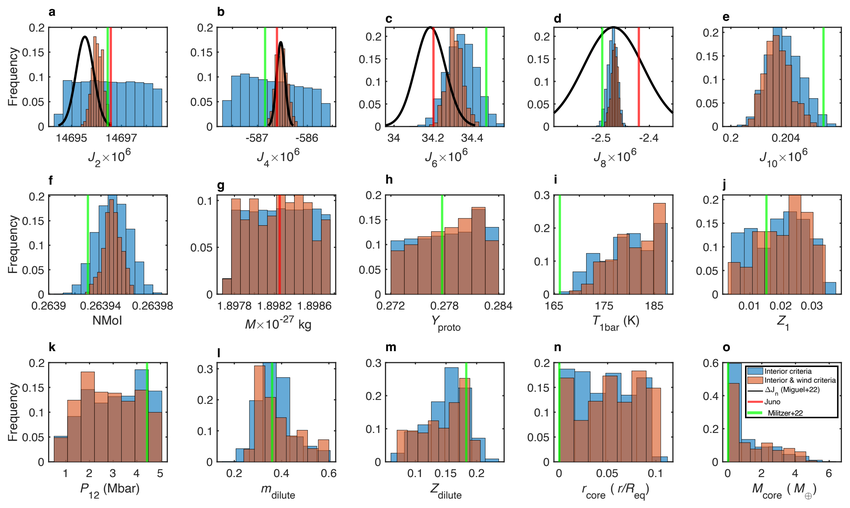

Figure 4 Distribution of the observables (**a-g**) and interior parameters (**h-n**) for plausible interior structures according to different criteria. M_{core} is the compact core mass.

Clustering analysis

- *k*-means clustering based on the 7 interior parameters
- Four clusters differentiate between the envelope and the core setups

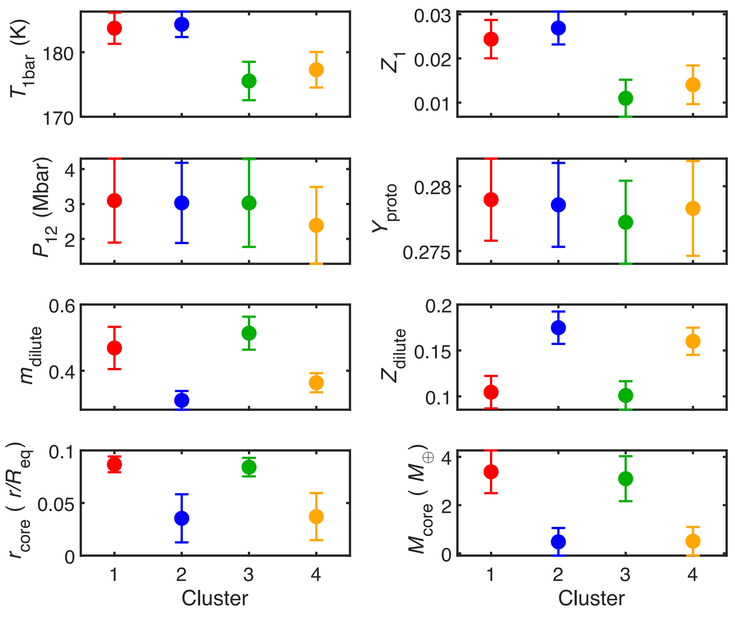

Figure 5 Means (points) and standard deviations (error bars) within the 4 clusters, shown in different colors. Clusters 1 and 2 (red and blue) show high values of T_{1bar} and Z_1, while clusters 3 and 4 (green and yellow) show lower values of these parameters. Clusters 1 and 3 feature high values of m_{dilute} and r_{core}, and low values of Z_{dilute}, whereas clusters 2 and 4 display the opposite trend. M_{core} was not used in the clustering analysis.

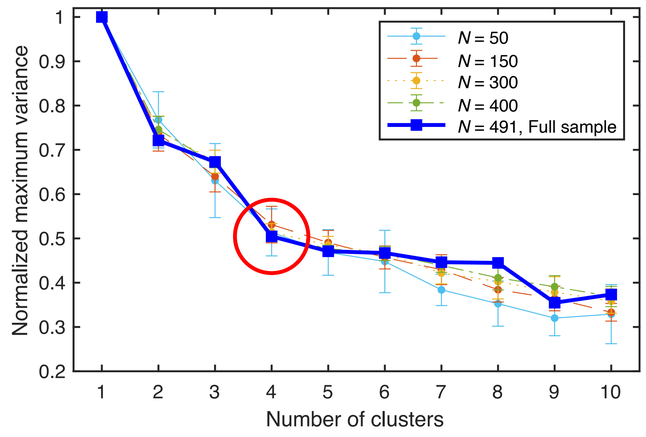

Figure 6 "Elbow analysis" for the full sample of plausible structures (thick blue), and the mean and σ of the analysis for 10 randomly selected samples of different size. The red circle marks the optimal number clusters

Results 2: Characteristic interior structures

- Jupiter's interior can be described by 2 effective parameters that clearly distinguish the 4 characteristic structures
- The overlap between clusters suggest that they are characteristic structures, not end members
- Most models constrained by the combination of $T_{1bar}\leq$178K, $Z_1\geq Z_{solar}$, and $P_{12}\leq$3Mbar falls within one key structure

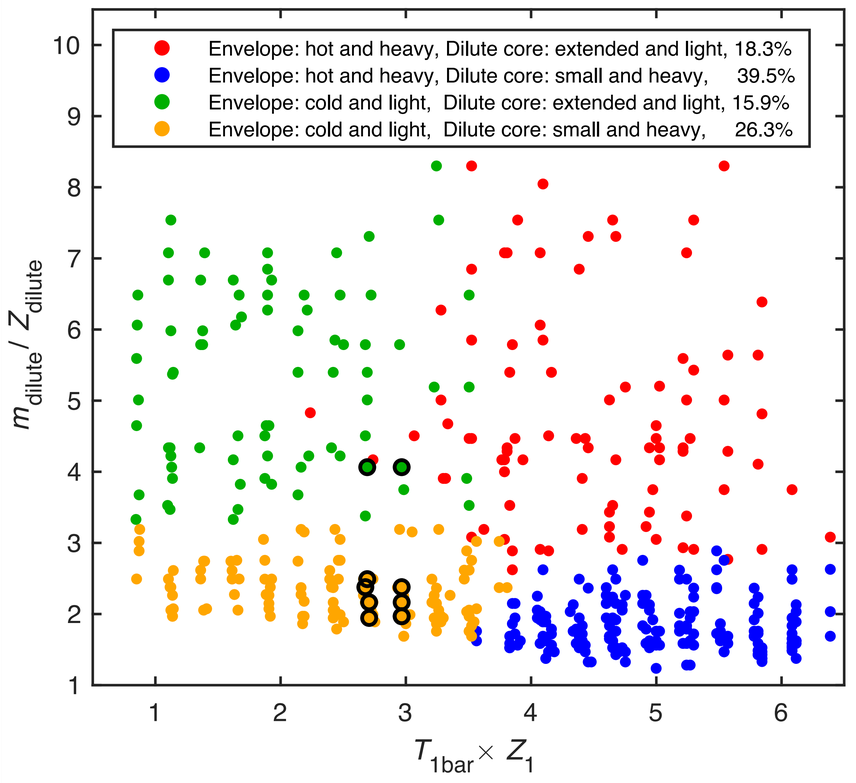

Figure 7 The plausible interior models in the phase space defined by the product of the two envelope-controlling parameters and the ratio of the two dilute core-controlling parameters. Black circles show the most observationally constrained interior models. The legend displays the fraction of models assigned to each cluster. "Heavy" and "light" refer to metallicity (molecular weight).

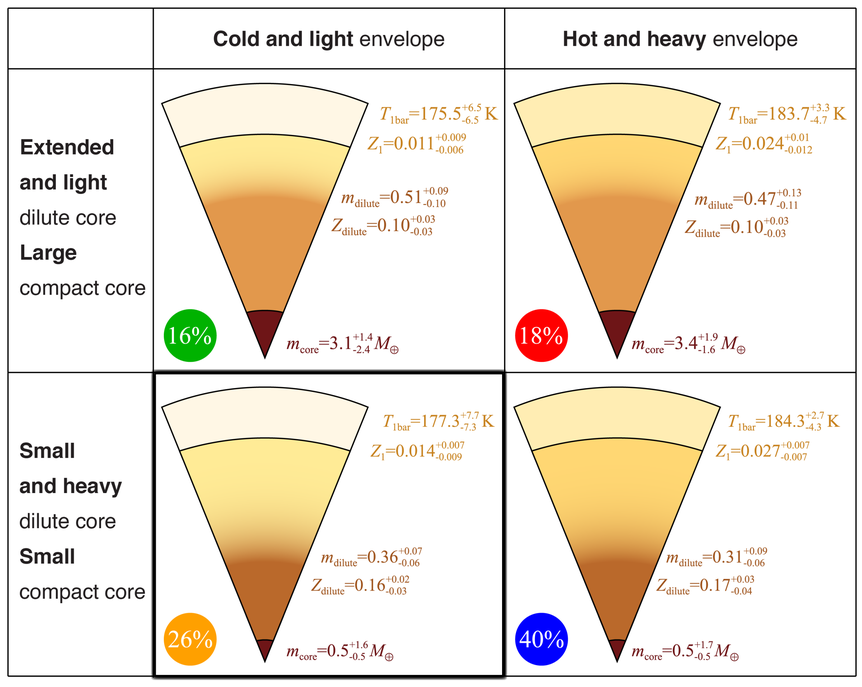

Figure 8 Schematic diagram of the four characteristic structures of Jupiter (not to scale).

References

- Chabrier, G., Mazevet, S., & Soubiran, F. 2019, ApJ, 872, 51 (CMS19)
- Durante, D., Parisi, M., Serra, D., et al. 2020, GRL, 47, e86572
- Galanti, E., Kaspi, Y., Miguel, Y., et al. 2019, GRL, 46, 616
- Howard, S. & Guillot, T. 2023, A&A, 672, L1 (HG23)
- Hubbard, W. B. 2013, ApJ, 768
- Miguel, Y., Bazot, M., Guillot, T., et al. 2022, A&A, 662, A18
- Militzer, B., Hubbard, W. B., Wahl, S., et al. 2022, PSJ., 3, 185